Formation of BaSi2 heterojunction solar cells using transparent MoO x hole transport layers

W. Du, R. Takabe, M. Baba, H. Takeuchi, K. O. Hara, K. Toko, N. Usami, and T. Suemasu

Citation: Applied Physics Letters **106**, 122104 (2015); doi: 10.1063/1.4916348
View online: http://dx.doi.org/10.1063/1.4916348
View Table of Contents: http://scitation.aip.org/content/aip/journal/apl/106/12?ver=pdfcov
Published by the AIP Publishing

Formation of $BaSi_2$ heterojunction solar cells using transparent MoO_x hole transport layers

W. Du,[1] R. Takabe,[1] M. Baba,[1] H. Takeuchi,[1] K. O. Hara,[2] K. Toko,[1] N. Usami,[3,4] and T. Suemasu[1,4]

[1]*Institute of Applied Physics, University of Tsukuba, 1-1-1 Tennohdai, Tsukuba, Ibaraki 305-8573, Japan*
[2]*Center for Crystal Science and Technology, University of Yamanashi, Yamanashi 400-8511, Japan*
[3]*Graduate School of Engineering, Nagoya University, Chikusa-ku, Nagoya 464-8603, Japan*
[4]*Core Research for Evolutionary Science and Technology, Japan Science and Technology Agency, Chiyoda, Tokyo 102-0075, Japan*

(Received 7 February 2015; accepted 17 March 2015; published online 27 March 2015)

Heterojunction solar cells that consist of 15 nm thick molybdenum trioxide (MoO_x, $x < 3$) as a hole transport layer and 600 nm thick unpassivated or passivated n-$BaSi_2$ layers were demonstrated. Rectifying current-voltage characteristics were observed when the surface of $BaSi_2$ was exposed to air. When the exposure time was decreased to 1 min, an open circuit voltage of 200 mV and a short circuit current density of 0.5 mA/cm^2 were obtained under AM1.5 illumination. The photocurrent density under a reverse bias voltage of −1 V reached 25 mA/cm^2, which demonstrates the significant potential of $BaSi_2$ for solar cell applications. © *2015 AIP Publishing LLC*.
[http://dx.doi.org/10.1063/1.4916348]

Thin-film solar cell materials such as CdTe, Cu(In,Ga)Se_2, Cu(In,Al)Se_2, and non-toxic alternatives such as Cu_2ZnSnS_4 have attracted much attention due to their high efficiency and low cost.[1–7] Perovskite-based solar cells have also gained increasing attention due to their rocket-like increase in efficiency and their simple fabrication process.[8,9] Thin-film Si solar cells have also been studied extensively for achieving high efficiencies by utilizing an efficient light-trapping system; however, it has been difficult to achieve efficiencies as high as 20%. Therefore, there is significant interest in other Si-based materials for thin-film solar cell applications. Among such materials, we have focused on barium disilicide ($BaSi_2$),[10,11] which is composed of abundant Si and Ba, and has a band gap of approximately 1.3 eV,[12,13] which matches that of the solar spectrum much better than crystalline Si. In spite of its indirect band gap, both theoretical and experimental studies have revealed that $BaSi_2$ has a large absorption coefficient exceeding 3×10^4 cm^{-1} for photon energies higher than 1.5 eV.[13–15] The large absorption coefficient originates from the band structure of $BaSi_2$, where the localized Ba *d*-like states form flat energy bands in the conduction band.[14–16] One of the most attractive features of $BaSi_2$ is that both the high absorption coefficient and large minority-carrier diffusion length can be utilized. This feature facilitates the collection of photogenerated carriers in an external circuit. Recent experimental results, such as the large minority-carrier diffusion length (ca. 10 μm)[17] and long minority-carrier lifetime (ca. 10 μs),[18,19] even in multidomain *a*-axis-oriented $BaSi_2$ epitaxial layers, have confirmed that $BaSi_2$ could be a candidate for thin-film solar cells. The six-fold symmetry of Si(111) means that *a*-axis-oriented $BaSi_2$ can be grown epitaxially on Si(111) with its three epitaxial variants rotating around the surface normal at 120° with respect to each other.[17] The grain size in $BaSi_2$ can be controlled from 0.1 to 4 μm, according to the growth conditions.[20] Grain boundaries (GBs) in polycrystalline semiconductors often degrade their electrical and optical properties. However, Kelvin probe force microscopy measurements indicate that the band structure at $BaSi_2$ GBs leads to repulsion of the minority carriers,[21–23] which reduces the charge carrier recombination at GBs. This band bending at GBs contributes to a long minority-carrier diffusion length in $BaSi_2$.

In this article, we demonstrate the solar cell performance for $BaSi_2$ heterojunction diodes based on 15 nm thick transparent substoichiometric molybdenum trioxide (MoO_x, $x < 3$) deposited on undoped n-$BaSi_2$ by thermal evaporation. In our previous studies, undoped $BaSi_2$ layers exhibited n-type conductivity with electron concentrations of approximately 10^{16}–10^{17} cm^{-3}.[12,24] Transition metal oxides have been studied extensively for the hole transport layer in organic solar cells and organic light emitting diodes, which has led to significant improvements in device performance and stability.[25,26] Javey's group applied MoO_x to crystalline Si (c-Si) solar cells and reported a conversion efficiency of 14.3% for an unpassivated MoO_x/n-c-Si solar cell and then 18.8% for a passivated MoO_x/a-Si:H/n-c-Si solar cell, in which the MoO_x layer functioned as a hole transport layer.[27,28] Undoped $BaSi_2$ also exhibits n-type conductivity and a work function that is smaller than that of n-Si;[29] therefore, we aimed to fabricate similar MoO_x/n-$BaSi_2$ structure solar cells by thermal evaporation of MoO_x on an unpassivated or passivated undoped n-$BaSi_2$ layer. Open circuit voltage (V_{OC}) and short circuit current density (J_{SC}) measurements of indium tin oxide (ITO)/MoO_x/n-$BaSi_2$ heterojunction diodes were then conducted under AM1.5 illumination.

An ion-pumped molecular beam epitaxy (MBE) system equipped with standard Knudsen cells for Ba and MoO_3, and an electron-beam evaporation source for Si was used for the growth of $BaSi_2$ films. First, the low resistivity n$^+$-Si substrate ($\rho < 0.01$ Ω cm) was heated at 900 °C for 30 min for thermal cleaning, and a thin $BaSi_2$ template layer was grown by reactive deposition epitaxy (RDE) at 500 °C for 5 min.

This template was used to control the crystal orientation of the $BaSi_2$ epitaxial overlayers.[30] Second, an approximately 600 nm thick *a*-axis-oriented undoped $BaSi_2$ layer was grown epitaxially by MBE at 600 °C for 8 h. The sample was then removed from the chamber and exposed to air to form a native oxide layer on the $BaSi_2$ (except for sample A) because long minority-carrier lifetime is ensured by the formation of oxides on the surface of $BaSi_2$.[31] The duration of exposure was 1 h, 5 min, and 1 min for samples B, C, and D, respectively. A 15 nm thick MoO_x ($x < 3$) layer was then formed on the $BaSi_2$ surface at room temperature (RT). Finally, 1 mm diameter, 200 nm thick ITO front electrodes were formed at RT by radio frequency (RF) magnetron sputtering using a mask. Al back contacts were also formed on the n-Si(111) substrate by RF sputtering. The sample cross section was observed using scanning electron microscopy (SEM). The crystalline quality of the films was evaluated by reflection high-energy electron diffraction (RHEED) and θ–2θ x-ray diffraction (XRD) measurements with a Cu Kα source. The photoresponse was evaluated using a lock-in technique that employed a xenon lamp with a 25 cm focal-length single monochromator (Bunko Keiki, SM-1700A). The electrical properties were characterized on the basis of current density versus voltage (*J*-*V*) and capacitance versus voltage (*C*–*V*) characteristics. The voltages were applied to the ITO electrode with respect to the n^+-Si substrate. *C*-*V* curves were measured by a parameter analyzer (Keysight B1500A) for frequencies ranging from 1 to 100 kHz. To investigate the grain size of $BaSi_2$, a 2 μm thick $BaSi_2$ layer was grown on Si(111) (sample E). The sample cross section was polished with a cross-section polisher using Ar ions, and electron backscatter diffraction (EBSD) measurement was performed. As described later, the grain size in $BaSi_2$ was approximately 2 μm. Thus, much thicker $BaSi_2$ layers than those in samples A–D were necessary. All the measurements were performed at RT.

Figures 1(a) and 1(b) show the RHEED patterns taken for sample A after growth of the $BaSi_2$ and MoO_x layers, respectively. The streaky RHEED pattern in Fig. 1(a) changed to the halo pattern in Fig. 1(b), which indicates that the MoO_x layer was amorphous. In the θ–2θ XRD pattern in Fig. 1(c), diffraction peaks were observed only from (100)-oriented $BaSi_2$ planes, such as (200), (400), and (600) planes, which indicates that the $BaSi_2$ epitaxial film was highly *a*-axis oriented. No diffraction peaks from ITO were observed, probably because of the amorphous MoO_x underlayer. Figure 1(d) shows a cross-sectional SEM image of sample A with the layered structure of ITO/MoO_x/$BaSi_2$/Si. Similar cross sections were observed for the other samples. To investigate the grain size in $BaSi_2$ and its crystal orientation in more detail, EBSD measurements of sample E were conducted.

Figure 2(a) shows a cross-sectional SEM image of sample E, and Figs. 2(b) and 2(c) present EBSD crystal orientation maps measured within the green rectangular area shown in Fig. 2(a) along the transverse direction (TD), and the direction between normal direction (ND) and reference direction (RD), respectively. The green color in Fig. 2(b) indicates that the $BaSi_2$ layer has the same (100) orientation in the surface normal as those in samples A-D. Figure 2(c),

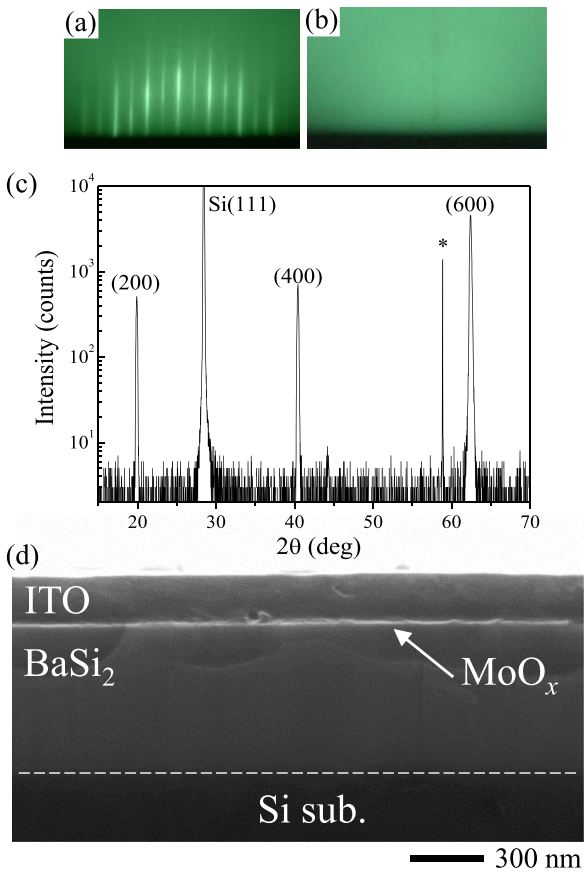

FIG. 1. RHEED patterns observed along Si[11$\bar{2}$] after the growth of (a) $BaSi_2$ and (b) MoO_x layers in sample A. (c) θ-2θ XRD pattern and (d) cross-sectional SEM image of sample A. The asterisk in (c) indicates the diffraction from the Si substrate.

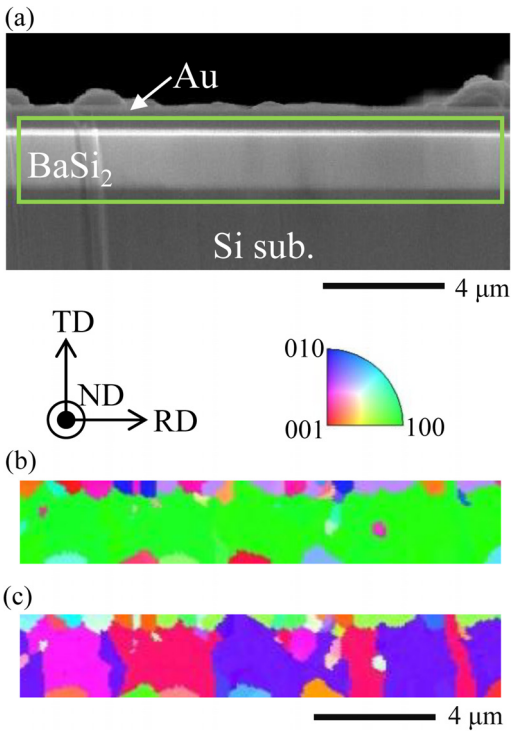

FIG. 2. (a) Cross-sectional SEM image of sample E, Au/$BaSi_2$ (2 μm)/Si(111). EBSD crystal orientation maps along the (b) TD and (c) the direction between ND and RD. The inset shows TD, RD, and ND, in addition to a color key.

where the different colors correspond to different grains, shows that the $BaSi_2$ grains have grown in the normal direction and the grain size is approximately 2 μm. Thus, it seems reasonable to think that the $BaSi_2$ grain size in samples A-D is as large as approximately 2 μm.

The *J-V* characteristics are discussed beginning with sample A, the ITO/MoO_x/$BaSi_2$ structure without air exposure. No rectifying properties were observed, as shown in Fig. 3(a), which is totally different to the situation reported for MoO_x/n-Si solar cells.[27,28] In contrast, rectifying *J-V* characteristics were observed for sample B, as shown in Fig. 3(b), in which the undoped $BaSi_2$ layer was exposed to air for a long time (1 h). This difference between samples A and B is attributed to the difference in the surface states of the undoped $BaSi_2$, i.e., exposure of the $BaSi_2$ surface to air or not. A large amount of surface defects, such as dangling bonds, may be present in the $BaSi_2$ surface region of sample A, which causes significant recombination at the MoO_x/$BaSi_2$ interface and thereby deteriorates the *J-V* characteristics. During air exposure, oxides such as SiO_x and BaO_x are likely to form, which function like a passivation layer on the surface of $BaSi_2$.[31] It was thus speculated that the *J-V* characteristics would therefore be improved in sample B. SiO_x is more likely to form because measurements using coaxial impact-collision ion scattering spectroscopy and atomic force microscopy suggest that the surface of *a*-axis-oriented $BaSi_2$ film grown on Si(111) is terminated by Si.[32] However, the formation of $BaSi_2$ surface oxides seems fast in air. Figure 3(b) shows that the forward *J* was very small in sample B; *J* started to increase after the bias voltage reached approximately 4 V. This small *J* was ascribed to the thick oxides on the $BaSi_2$ surface, which block the current flow at the MoO_x/$BaSi_2$ interface. Therefore, to decrease the thickness of this oxide layer, the exposure duration was shortened from 1 h to 5 min (sample C). Figure 3(c) shows the *J-V* characteristics for sample C under dark and illumination (AM1.5) conditions. The photocurrent was observed under reverse bias conditions. The photocurrent density J_L started to increase at a reverse bias voltage, $V \approx -0.3$ V, and became saturated at approximately 25 mA/cm^2 with $V \approx -1$ V. According to the total number of photons above 1.3 eV in the AM1.5 spectrum, the maximum J_L is estimated to be approximately 30 mA/cm^2.[33] J_L for the 600 nm thick $BaSi_2$ active layer reached 25 mA/cm^2; therefore, this material has significant potential for thin-film solar cell applications. However, in the present device, J_L decreased down to 0 for $V > -0.3$. It was speculated that the oxide layer was still sufficiently thick for photogenerated carrier transport. Therefore, the duration of air exposure was further shortened from 5 min to 1 min (sample D).

Figure 3(d) shows typical *J-V* characteristics for sample D under dark and illumination conditions. V_{OC} is approximately 200 mV and J_{SC} is around 0.5 mA/cm^2. The external quantum efficiency (EQE) obtained by the built-in electric field in the MoO_x/n-$BaSi_2$ junction, i.e., $V = 0$ in Fig. 4, showed a peak value of 3% at 2.0 eV. The EQE began to increase sharply for photon energies larger than 1.3 eV, which is in good agreement with the band gap of $BaSi_2$ and our previous results.[34,35] The valley-like structure at around 2.5 eV (ca. 500 nm) in the spectrum was caused by light interference in the ITO layer. Although these values (V_{OC}, J_{SC}, and EQE) are still very small and far from the requirements for a solar cell, they provide strong evidence that $BaSi_2$ is a very promising material for thin-film solar cell applications. The EQE increased significantly under small reverse bias voltages, as shown in Fig. 4. The peak EQE reached approximately 55% at −0.5 V and 75% at −1 V, which indicates that the electric field stretched into the undoped $BaSi_2$ layer under reverse bias voltages and photogenerated carriers were

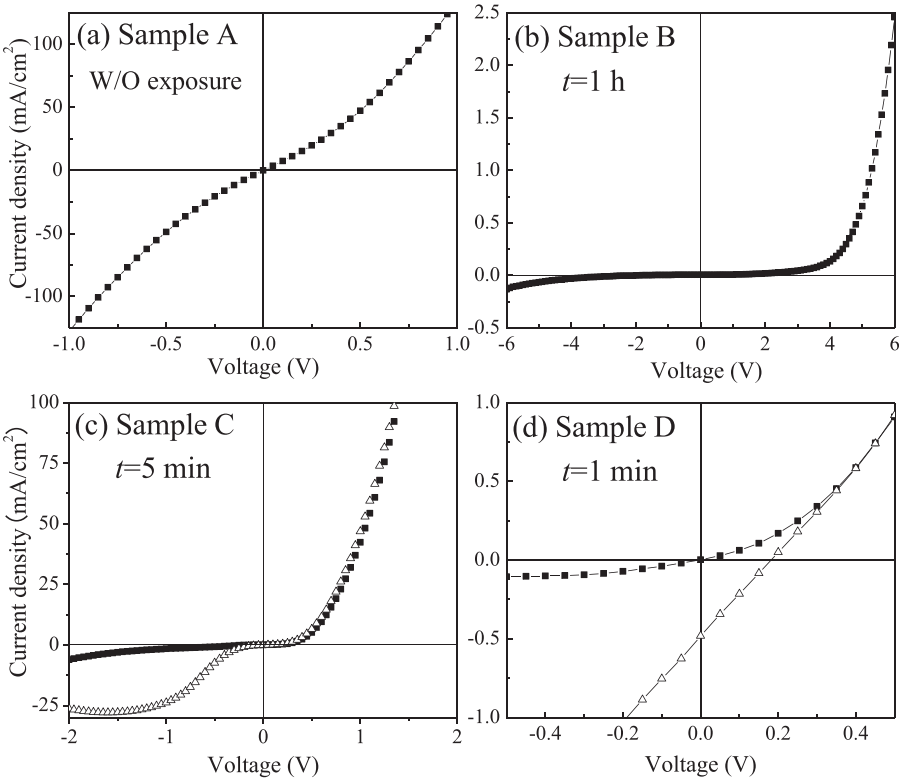

FIG. 3. *J-V* characteristics for samples (a) A, (b) B, (c) C, and (d) D under dark and illumination (AM1.5) conditions. The bias voltage was applied to the ITO with respect to the n^+-Si. The duration *t* of $BaSi_2$ exposure to air was 0, 1 h, 5 min, and 1 min for samples A-D, respectively.

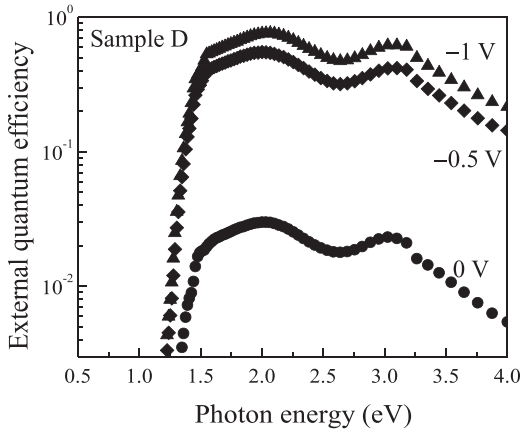

FIG. 4. EQE for sample D under various bias voltages: $V = 0$, -0.5, and -1.0 V.

extracted efficiently. This phenomenon was mainly due to the short minority-carrier lifetime in the undoped $BaSi_2$ layer caused by incomplete passivation of the $BaSi_2$ surface.

C-V curves for samples B-D are presented in Fig. 5 to discuss electron traps at the $MoO_x/BaSi_2$ interface. The measurement frequency was varied from 1 to 100 kHz. With increasing the bias voltage, the capacitance increases. This is because the majority carriers (electrons) are accumulated at the native oxide/n-$BaSi_2$ interface as in the case of a metal-oxide-silicon diode.[36] It is considered that some of the electrons are trapped at the $BaSi_2$ surface states. The measured capacitance is a series combination of the capacitance related to defect states at the interface and the others related to oxides. The former is much smaller than the others; therefore, it is safe to state that the measured capacitance roughly reflects the capacitance related to the defect states at the interface. At lower frequencies, the $BaSi_2$ surface states can follow the ac voltage swing; therefore, the capacitance increases with decreasing frequencies. The fact that capacitances are smaller for sample B, in which the $BaSi_2$ surface was exposed to air for a longer time than those in samples C and D, suggests that the air exposure reduces the trapped electrons; thereby, the surface defect states of $BaSi_2$. At present, the formation of oxides on the $BaSi_2$ surface is highly dependent on many parameters, such as exposure duration,

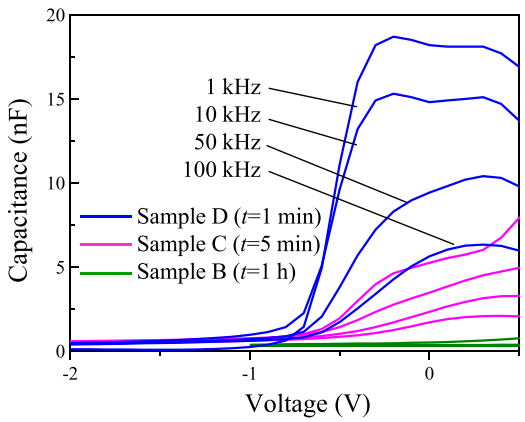

FIG. 5. *C-V* curves for samples B-D. The measurement frequency was varied as 1, 10, 50, and 100 kHz. The bias voltage was applied to the ITO with respect to the n^+-Si.

temperature, and humidity. Therefore, a reliable means to achieve both sufficient surface passivation and formation of a thin passivation (oxide) layer is still required.

In summary, an ITO (200 nm)/MoO_x (15 nm)/n-$BaSi_2$ (600 nm) heterojunction solar cell was fabricated by thermal evaporation of a 15 nm thick MoO_x layer. When the $BaSi_2$ surface was exposed to air for 1 min to achieve surface passivation, rectifying *J-V* characteristics were observed at RT. Solar cell performance with $V_{OC} = 200$ mV and $J_{SC} = 0.5$ mA/cm^2 was obtained under AM1.5 illumination. J_L was saturated at approximately 25 mA/cm^2 when the bias voltage was -1 V. Rectifying *J-V* characteristics were ensured by longer exposure of the $BaSi_2$ to air; however, *J* was then decreased due to thicker oxide formation, which blocked the current flow. Thus, control of the passivation process with more precision would enable the efficiency of $BaSi_2$ solar cells to be improved.

C-V measurements were conducted with the help of Professor R. Hasunuma of the University of Tsukuba. This work was financially supported in part by the Core Research for Evolutionary Science and Technology (CREST) of the Japan Science and Technology Agency (JST).

[1]B. M. Basol, J. Appl. Phys. **55**, 601 (1984).
[2]M. A. Green and S. R. Wenham, Appl. Phys. Lett. **65**, 2907 (1994).
[3]W. Jaegermann, A. Klein, and T. Mayer, Adv. Mater. **21**, 4196 (2009).
[4]S. Ahmed, K. B. Reuter, O. Gunawan, L. Guo, L. T. Romankiw, and H. Deligianni, Adv. Eng. Mater. **2**, 253 (2012).
[5]H. Katagiri, K. Jimbo, W. S. Maw, K. Oishi, M. Yamazaki, H. Araki, and A. Takeuchi, Thin Solid Films **517**, 2455 (2009).
[6]M. Banavoth, S. Dias, and S. B. Krupanidhi, AIP Advances **3**, 082132 (2013).
[7]B. Murali and S. B. Krupanidhi, Dalton Trans. **43**, 1974 (2014).
[8]M. A. Green, A. Ho-Baillie, and H. J. Snaith, Nat. Photonics **8**, 506 (2014).
[9]H. S. Kim, S. H. Im, and N. G. Park, J. Phys. Chem. C **118**, 5615 (2014).
[10]J. Evers, G. Oehlinger, and A. Weiss, Angew. Chem., Int. Ed. **16**, 659 (1977).
[11]M. Imai and T. Hirano, J. Alloys Compd. **224**, 111 (1995).
[12]K. Morita, Y. Inomata, and T. Suemasu, Thin Solid Films **508**, 363 (2006).
[13]K. Toh, T. Saito, and T. Suemasu, Jpn. J. Appl. Phys., Part 1 **50**, 068001 (2011).
[14]D. B. Migas, V. L. Shaposhnikov, and V. E. Borisenko, Phys. Status Solidi B **244**, 2611 (2007).
[15]M. Kumar, N. Umezawa, and M. Imai, Appl. Phys. Express **7**, 071203 (2014).
[16]Y. Imai, A. Watanabe, and M. Mukaida, J. Alloys Compd. **358**, 257 (2003).
[17]M. Baba, K. Toh, K. Toko, N. Saito, N. Yoshizawa, K. Jiptner, T. Sakiguchi, K. O. Hara, N. Usami, and T. Suemasu, J. Cryst. Growth **348**, 75 (2012).
[18]K. O. Hara, N. Usami, K. Toh, M. Baba, K. Toko, and T. Suemasu, J. Appl. Phys. **112**, 083108 (2012).
[19]K. O. Hara, N. Usami, K. Nakamura, R. Takabe, M. Baba, K. Toko, and T. Suemasu, Appl. Phys. Express **6**, 112302 (2013).
[20]M. Baba, K. Nakamura, W. Du, M. Ajmal Khan, S. Koike, K. Toko, N. Usami, N. Saito, N. Yoshizawa, and T. Suemasu, Jpn. J. Appl. Phys. **51**, 098003 (2012).
[21]M. Baba, S. Tsurekawa, K. Watanabe, W. Du, K. Toko, K. O. Hara, N. Usami, T. Sekiguchi, and T. Suemasu, Appl. Phys. Lett. **103**, 142113 (2013).
[22]M. Baba, K. O. Hara, D. Tsukahara, K. Toko, N. Usami, T. Sekiguchi, and T. Suemasu, J. Appl. Phys. **116**, 235301 (2014).
[23]D. Tsukahara, M. Baba, S. Honda, Y. Imai, K. O. Hara, N. Usami, K. Toko, J. H. Werner, and T. Suemasu, J. Appl. Phys. **116**, 123709 (2014).

[24]W. Du, M. Baba, K. Toko, K. O. Hara, K. Watanabe, T. Sekiguchi, N. Usami, and T. Suemasu, J. Appl. Phys. **115**, 223701 (2014).
[25]V. Shrotriya, G. Li, Y. Yao, C. Chu, and Y. Yang, Appl. Phys. Lett. **88**, 073508 (2006).
[26]M. T. Greiner, M. G. Helander, W. Tang, Z. Wang, J. Qiu, and Z. Lu, Nat. Mater. **11**, 76 (2012).
[27]C. Battaglia, X. Yin, M. Zheng, I. D. Sharp, T. Chen, S. McDonnell, A. Azcatl, C. Carraro, B. Ma, R. Maboudian, R. M. Wallace, and A. Javey, Nano Lett. **14**(**2**), 967 (2014).
[28]C. Battaglia, S. M. de Nicolaś, S. De Wolf, X. Yin, M. Zheng, C. Ballif, and A. Javey, Appl. Phys. Lett. **104**, 113902 (2014).
[29]T. Suemasu, K. Morita, M. Kobayashi, M. Saida, and M. Sasaki, Jpn. J. Appl. Phys., Part 2 **45**, L519 (2006).
[30]Y. Inomata, T. Nakamura, T. Suemasu, and F. Hasegawa, Jpn. J. Appl. Phys., Part 2 **43**, L478 (2004).
[31]R. Takabe, K. O. Hara, M. Baba, W. Du, N. Shimada, K. Toko, N. Usami, and T. Suemasu, J. Appl. Phys. **115**, 193510 (2014).
[32]S. Okasaka, O. Kubo, D. Tamba, T. Ohashi, H. Tabata, and M. Katayama, Surf. Sci. **635**, 115 (2015).
[33]C. H. Henry, J. Appl. Phys. **51**, 4494 (1980).
[34]Y. Matumoto, D. Tsukahara, R. Sasaki, M. Takeishi, and T. Suemasu, Appl. Phys. Express **2**, 021101 (2009).
[35]W. Du, M. Suzuno, M. Ajma Khan, K. Toh, M. Baba, K. Nakamura, K. Toko, N. Usami, and T. Suemasu, Appl. Phys. Lett. **100**, 152114 (2012).
[36]S. M. Sze, *Physics of Semiconductor Devices*, 2nd ed. (Wiley, New York, 1981), Chap. 7.